2017 IEEE-RAS 17th International Conference on
Humanoid Robotics (Humanoids)
Birmingham, UK, November 15-17, 2017

# Investigations of Viscoelastic Liquid Cooled Actuators Applied for Dynamic Motion Control of Legged Systems

Donghyun Kim[1], Orion Campbell[1], Junhyeok Ahn[1], Luis Sentis[2] and Nicholas Paine[3]

***Abstract*— To significantly improve actuation technology for legged systems, we design, build, and empirically test the viscoelastic liquid cooled actuator (VLCA) for use in a robotic leg. Unlike existing actuators, VLCAs excel in the following five critical axes of performance, which are essential for dynamic motion control of practical legged robots: energy efficiency, power density, impact-resistance, position controllability, and force controllability. In this paper, we explain design details with respect to the five criteria, and present results from our extensive study of a variety of viscoelastic materials. Position controllability and power density are experimentally evaluated by demonstrating dynamic motion with a single leg testbed, custom-built using VLCAs. In the experiment, the testbed shows $6.1\ \mathrm{rad/s}$ maximum velocity and $240\ \mathrm{N\,m}$ maximum torque while accurately executing the commanded motions.**

## I. INTRODUCTION

Bipedal robots are alternatives to wheeled platforms due to their maneuverability in various terrains, their small footprint for operations in tight spaces, and their omnidirectional movements. However, to be a practical tool for humans, several critical issues must be addressed. A bipedal system must be robust to external disturbances, especially impact from ground. Moreover, it must be energy-efficient, powerful, and agile to execute a variety of required tasks such as exploring urban environments, carrying heavy loads, or walking and running over irregular terrains. To be a reliable and useful mobile platform, robots also need to provide high-quality position and force feedback control. However, achieving impact-resistance, energy efficiency, power density, and controllability simultaneously is a technical challenge and needs significant engineering effort to improve current state-of-the-art actuator design.

Existing actuators can be categorized using four criteria: power source (electric or hydraulic), cooling type (air or liquid), elasticity of the drivetrain (rigid or elastic), and drivetrain type (direct, harmonic drive, ball screw, etc.) [1], [2]. One of the most powerful and common solutions is a hydraulic, liquid-cooled, rigid, and direct drive actuator, with a high power-to-weight ratio, torque-to-weight ratio, position controllability, and shock tolerance. Existing robots that use this type of actuator include Atlas, Spot, Big Dog, and Wildcat of Boston Dynamics, BLEEX of Berkeley [3], and HyQ of IIT [4], [5]. However, hydraulics are less energy efficient primarily because they require more energy transformations [6]. Typically, a gasoline engine or electric motor spins a pump, which compresses hydraulic fluid, which is modulated by a hydraulic servo valve, which finally causes a hydraulic piston to apply a force. Each stage in this process incurs some efficiency loss, and the total losses can be very significant.

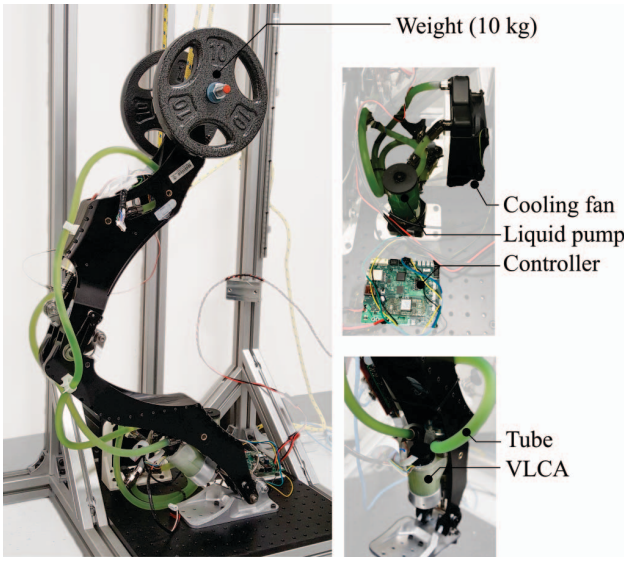


Fig. 1. **Single leg testbed.** Our testbed consists of two VLCAs at the ankle and the knee.

Electric, air-cooled, rigid, and harmonic drive actuators are other widely used actuation types. Some robots utilizing these actuator types include Asimo of Honda, HRP2,3,4 of AIST [7], HUBO of KAIST [8], REEM-C of PAL Robotics, JOHNNIE and LOLA of Tech. Univ. of Munich [9], [10], Robosimian of NASA JPL [11], and more. These actuators have precise position control and high torque density. Additionally, they are significantly more energy efficient when compared to hydraulic actuation. On the other hand, low shock tolerance, low fidelity force sensing, and low efficiency gearboxes are common drawbacks of these actuators. According to Harmonic Drive AGs catalog, the efficiency of harmonic drives may be as poor as 25% and only increases above 80% when optimal combinations of input shaft speed, ambient temperature, gear ratio, and lubrication are present.

[12] used liquid cooling for electric, rigid, harmonic drive actuators to enhance continuous power-to-weight ratio. The robots using this type of actuation include SCHAFT and JAXON [13]. These actuators share the advantages and

[1]D. Kim, O. Campbell, J. Ahn are with the Graduate School of Mechanical Engineering, University of Texas at Austin, U.S.

[2]Luis Sentis is associate professor in Aerospace Engineering and Engineering Mechanics, University of Texas at Austin, U.S. lsentis@austin.utexas.edu

[3]Nicholas Paine is the Chief Technology Officer of Apptronik, Austin, U.S. npaine@apptronik.com

Nicholas Paine and Luis Sentis are corresponding for the presented work

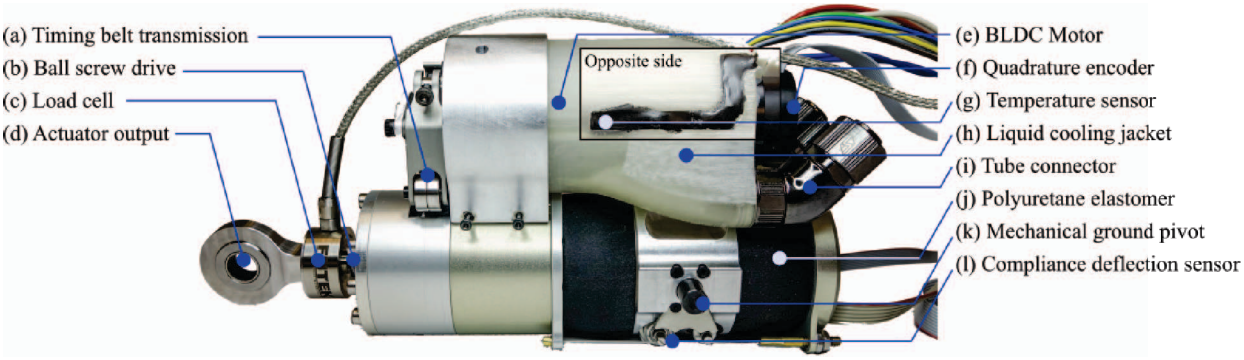


Fig. 2. **Viscoelastic Liquid Cooled Actuator.** The labels are explanatory. In addition, the actuator contains five sensors: a load cell, a quadrature encoder for the electric motor, a temperature sensor, and two rubber deflection sensors. One of the rubber deflection sensors is absolute and the other one is a quadrature encoder. The quadrature encoder gives high quality velocity data of the rubber deflection.

disadvantages of electric, rigid, harmonic drive actuators, but have a significant increase of the continuous power output and torque density. One of our studies [14], indicates a 2x increase in sustained power output by retrofitting an electric motor with liquid cooling. Other published results indicate a 6x increase in torque density through liquid cooling [1], [15], though such performance required custom-designing a motor specifically for liquid cooling. In our case we use an off-the-shelf electric motor.

Although the increased power density achieved via liquid cooling amplifies an electric actuators' power, the rigid drivetrain is still vulnerable to external impacts, which are common in dynamic locomotion. To improve the impact tolerance, many robots (e.g. WALK-MAN [16] and COMAN of IIT [17], Valkyrie of NASA [18], MABEL and MARLO in UMich [19], [20], StarlETH of ETH [21], and a biped with elastomer-based SEAs [22]) adopt electric, air-cooled, elastic, harmonic drive actuators. This type of actuation provides high quality force sensing, force control, impact resistance, and energy efficiency. However, precise position control is difficult because of the elasticity in the drivetrain and the coupled effect of force feedback control and realtime latencies [23]. Low efficiency originating from the harmonic drives is another drawback.

As an alternative to harmonic drives, ball screws are great drives for mechanical power transmission. SAFFiR, THOR, and ESCHER of Virginia Tech [24]–[26], M2V2 of IHMC [27], Spring Flamingo of MIT [28], Hume of UT Austin [29], and the X1 Mina exoskeleton of NASA [30] use electric, air-cooled, elastic, ball-screw drives. These actuators show energy efficiency, good power and force density, low noise force sensing, high fidelity force controllability, and low backlash. However, most ball screw configurations make the actuator bulky. Another drawback is poor position controllability caused by the elastic elements. There are some other actuators that have special features such as the electric actuators used in MIT's cheetah [31], which allow for shock resistance through a transparent but backlash-prone drivetrain. In summary, nearly all existing actuators have at least one critical drawback with respect to the dynamic motion control of legged systems.

To address efficiency, impact resistance, increased continuous and instantaneous power and torque density, position and force controllability, we propose a novel viscoelastic liquid-cooled actuator (VLCA) and use it in a prototype leg. To obtain both impact resistance and position controllability, we use rubber viscoelastic elements instead of metal springs. To maintain the high fidelity force control of series elastic actuators, we extensively studied the properties of viscoelastic materials and found that polyurethane has high linearity (0.992), low compression set (2%), and low creep (15%). Liquid cooling is another important aspect of our actuator, which significantly enhances the continuous and instantaneous power and torque density. For efficiency, we use brushless DC motors and a compact ball-screw assembly.

In order to test this novel design, we devise a two degree-of-freedom (DOF), single leg testbed, shown in Fig. 1. This testbed integrated two of the new actuators, one in the ankle, and another in the knee, while restricted motions to the sagittal plane. With the foot bolted to the floor for initial tests, weight plates can be loaded on the hip joint to serve as an end-effector payload. We test a variety of cartesian space trajectories and use inverse kinematics to compute joint trajectories. Our control model employed both a feedforward and feedback term to reduce the position error. Feedforward forces were computed from joint trajectories along with the inertial characteristics of the testbed and reflected through the linkage transformation and into a feedforward motor current using a 90% motor efficiency constant. Overall, our contributions include 1) designing a novel actuator, dubbed VLCA, 2) extensively studying the viscoelastic properties, and 3) studying the performance of the actuators in a multi-dof leg prototype.

## II. Viscoelastic Liquid Cooled Actuation

The design objectives of the VLCA can are 1) power density, 2) efficiency, 3) impact tolerance, 4) position controllability, and 5) force controllability. To achieve fast dynamic motions, we optimized the actuator to achieve 0.7 $\mathrm{N\,m}$ of motor continuous torque. In [14], the authors achieve a significant improvement in motor current, torque, output power and system efficiency for liquid cooled commercial off-the-

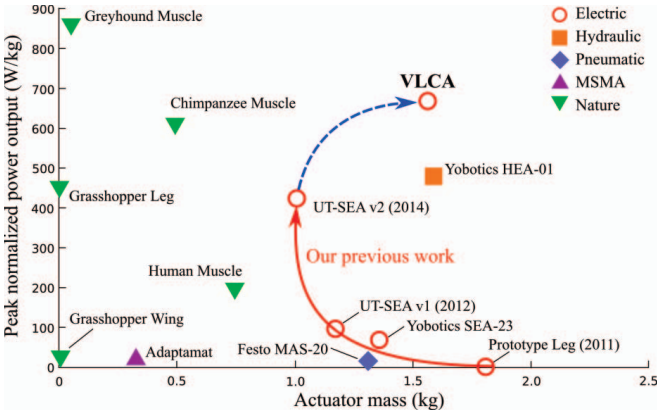


Fig. 3. **Experimentally validated peak power densities of several actuation technologies.** Advancing upon our previous UT-SEA [32] technology, the graph illustrates a potential trend towards high power performance of electric actuators.

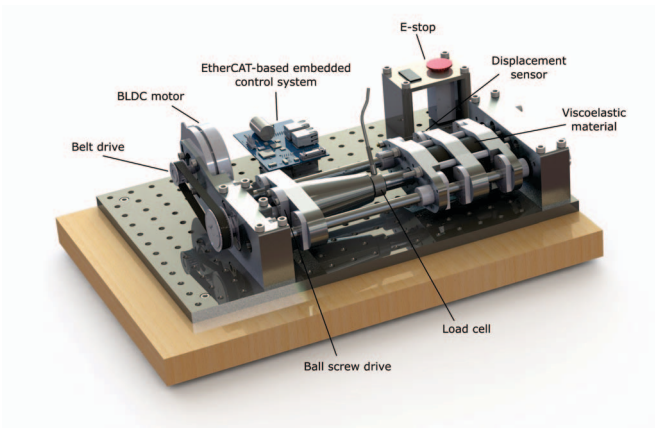


Fig. 4. **Viscoelastic material testbed** The testbed shown here (a real embodiment also exists) was designed and constructed to study various material properties of candidate viscoelastic materials and to begin evaluating expected control performance techniques. The development of this testbed reduces the technological risk associated with engineering viscoelastic systems.

shelf (COTS) electric motors and studied several Maxon motors for comparison. As an extension of this previous work, in this new study we studied COTS motors and their thermal behavior models and selected the Maxon EC-max 40 brushless 120 W (Fig. 2(e)), with a custom housing designed for the liquid cooling system (Fig. 2(h)). Finally, a thermal ratio of 3.59 (defined as the improvement on the continuous current) and a continuous motor torque of 0.701 $\mathrm{N\,m}$ are theoretically achievable. Energetically, this actuator is designed to achieve 366W continuous power output with an 85% ball screw efficiency (Fig. 2(b)). With the total actuator mass of 1.692kg, this translates into a continuous power of 216W and peak power of 650W (Fig. 3). The combined effect of convection liquid cooling, high power brushless DC (BLDC) motors, and a high-efficiency ball screw aims at surpassing existing electric actuation technologies with COTS motors in terms of power density (Fig. 3).

BLDC motors typically obtain peak efficiencies of around 90% while ball screws also obtain efficiencies of around 90%. The overall system efficiency from the power source to the mechanical output of the actuator has been measured at around 55% for a similar system [2]. In contrast, the efficiency of hydraulic systems is typically around 15%.

For legged robots, impact occurs frequently and is likely to damage rigid, electric actuator designs. Such architectures are susceptible to impact loads due to the combined effects of large rotor inertia (a result of the gearbox speed reduction) and no drive train compliance. On the other hand, impact tolerance is a key advantage of SEAs due to the compliance in the drive train. VLCAs retain this impact resistance property via the use of a viscoelastic component in series with the actuator output.

In terms of controls, a common problem with conventional SEAs is their lack of physical damping at their mechanical output. As a result, active damping must be provided from torque produced by the motor [33]. However, the presence of signal latency and derivative signal filtering limit the amount by which this active damping can be increased, resulting in SEA driven robots achieving only relatively low output impedances [23] and thus operating with limited position control accuracy and bandwidth. Our VLCA design incorporates damping directly into the compliant element itself, reducing the requirements placed on active damping efforts from the controller. The incorporation of passive damping aims at increasing the output impedance while retaining compliance properties, resulting in higher position control bandwidth. The material properties we took into consideration will be introduced in Section III. The retention of a compliant element in the VLCA drive means that deflection based measurement of actuator forces is enabled. The inclusion of a load cell (Fig. 2(c)) on the actuators output serves as a redundant force sensor and is used to calibrate the force displacement characteristics of the viscoelastic element.

Mechanical power is transmitted when the motor turns a ball nut via a low-loss timing belt and pulley (Fig. 2 (a)), which causes a ball screw to apply a force to the actuators output (Fig. 2(d)). The rigid assembly consisting of the motor, ball screw, and ball nut connects in series to a compliant viscoelastic element (Fig. 2(j)), which connects to the mechanical ground of the actuator (Fig. 2(k)). When the actuator applies a force, reaction forces compress the viscoelastic element. The viscoelastic element enables the actuator to be more shock tolerant than rigid actuators yet also maintain high output impedance due to the inherent damping in the elastomer.

## III. VISCOELASTIC MATERIAL CHARACTERIZATION

Our main objective in using elastomers instead of metal springs is to benefit from their intrinsic damping properties. However, the mechanical properties of viscoelastic materials are difficult to predict, thus making the design of an actuator based on these materials a challenge.

The most challenging aspect of incorporating elastomers into the structural path of an actuator is in estimating or modeling their complex mechanical properties. Elastomers pos-

| Materials | Hardness (A) | Tensile Strength (kPa) | Material Cost ($) |
|---|---|---|---|
| High-temperature silicone | 90 | 5170 | 29.41 |
| Fabric-reinforced silicone | 70 | 8960 | 29.08 |
| Ultra-strength oil-resistance Buna-N | 90 | 24130 | 51.47 |
| Viton Fluoroelastomer | 75 | 10340 | 105.62 |
| High-strength weather resistance EPDM | 80 | 10340 | 35.28 |
| Abrasion-resistance polyurethane | 80 | 43780 | 19.40 |
| Abrasion-resistance polyurethane | 90 | 37920 | 19.40 |

TABLE I

VISCOELASTIC MATERIAL CANDIDATES

sess both hysteresis and strain-dependent stress, which result in nonlinear force displacement characteristics. Additionally, elastomers also exhibit time-varying stress-relaxation effects when exposed to a constant load. The result of this effect is a gradual reduction of restoration forces when operating under a load. A third challenge when using elastomers in compression is compression set. This phenomenon occurs when elastomers are subjected to compressive loads over long periods of time. An elastomer that has been compressed will exhibit a shorter free-length than an uncompressed elastomer. Compression set is a common failure mode for o-rings and in our application could lead to actuator backlash if not accounted for properly.

To address these various engineering challenges we designed experiments to empirically measure the following four properties of our viscoelastic springs: 1) force versus displacement, 2) stress relaxation, 3) compression set, and 4) frequency response, which will be used to characterize each material's effective viscous damping. We built a viscoelastic material testbed, depicted in Fig. 4, to measure each of these properties. We selected and tested the seven candidate materials that are listed in Table I.

### A. Force versus displacement

In the design of compliant actuation, it is essential to know how much a spring will compress given an applied force. This displacement determines the required sensitivity of a spring-deflection sensor and also affects mechanical aspects of the actuator such as usable actuator range of motion and clearance to other components due to Poisson ratio expansion. In this experiment (see supplementary video), we identify the force versus displacement curves for the various elastomer springs and experimental data for all eight springs as shown in Fig 5. One point to be noted is that there is a disagreement between our empirical measurements and the analytic model relating stiffness to hardness, i.e. the Gent's relation shown in [34]. This mismatch arises because in our experiments the materials are preloaded whereas the analytical models assume unloaded materials.

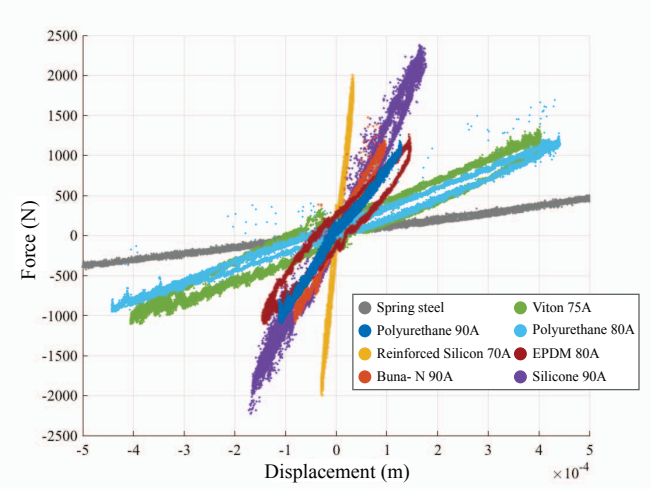


Fig. 5. **Force versus displacement curves** A strong correlation between material hardness and the materials stiffness can be observed. An exception to this correlation is the fabric reinforced silicone which we hypothesize had increased stiffness due to the inelastic nature of its reinforcing fabric. Nonlinear effects such as hysteresis can also be observed in this dataset.

### B. Stress relaxation

Stress-relaxation is an undesirable property in compliant actuators for two reasons. First, the time-varying force degrades the quality of the compliant material as a force sensor. When a material with significant stress-relaxation properties is used, the only way to accurately estimate actuator force based on deflection data is to model the effect and then introduce deflection data through this model to obtain a force estimate. This model introduces complexity and more room for error. The second reason stress-relaxation can be problematic is that it can lead to the loss of contact forces in compression-based spring structures. Empirically measured stress-relaxation properties for each of the materials are shown in Fig. 6.

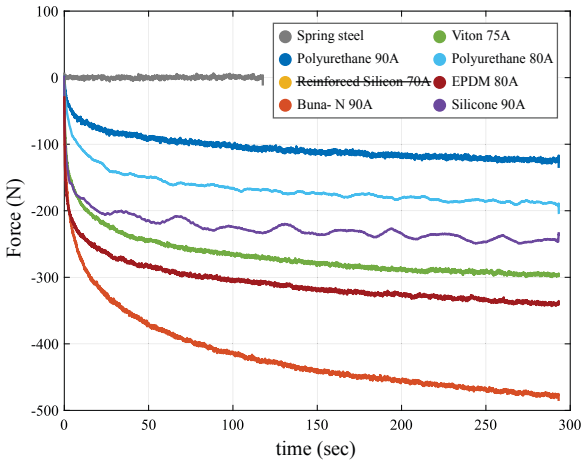


Fig. 6. **Stress relaxation comparison curves for all of the tested materials.** We created a set of experiments which command a rapid change in material displacements and then measured the materials force (deformation) versus time for 300 seconds.

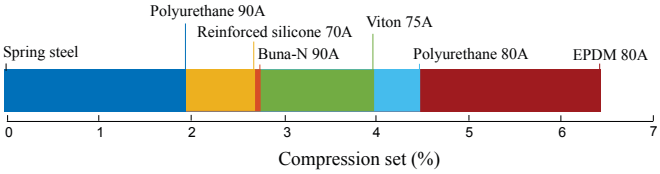


Fig. 7. **Comparison of compression set properties for viscoelastic materials.** We measured each elastomers free length both before and after the spring was placed in the preloaded test-bed.

| Spring | Natural frequency (Hz) | Damping ratio | Total damping (Drive train and compliant element) (N s/m) | Compliance damping (N s/m) |
|---|---|---|---|---|
| Metal | 3.6 | 0.1 | 8000 | 0 |
| Poly 80A | 6.0 | 0.1 | 12000 | 4000 |
| Silicone 90A | 9.4 | 0.1 | 37000 | 37000 |

TABLE II
DAMPING OF ELASTOMERS

### C. Compression set

Compression set is the reduction in length of an elastomer after prolonged compression. The drawback of using materials with compression set in compliant actuation is that the materials must be installed with larger amounts of preload forces to avoid the material sliding out of place during usage. To measure this property, we measured each elastomers free length both before and after the elastomer was placed in the preloaded testbed. The result of our compression set experiments are summarized in Fig. 7.

### D. Dynamic response

With regards to compliant actuation, the primary benefit of using an elastomer spring is its viscous properties, which can characterize the dynamic response of an actuator in series with such a component. To perform this experiment, we generate motor current to track an exponential chirp signal, testing frequencies between 0.001Hz and 200Hz. Given the input-output relation of the system, we can fit a second order transfer function to the experimental data to obtain an estimate of the systems viscous properties. However, this measure also includes the viscoelastic testbed's ballscrew drive train friction (Fig. 4). To quantify the elastomer spring damping independent of the damping of the testbed drive train, the metal die spring (8000 $\mathrm{N\,s/m}$) was first characterized, and then subtracted from subsequent tests of the elastomer springs to obtain estimates for the viscous properties of the elastomer materials. Fig. 8 shows the frequency response results of four different springs, while controlling the damping ratio. The elastomers have higher stiffness than the metal spring, hence their natural frequencies are higher. Table II shows the measured damping calculated for the two elastomers.

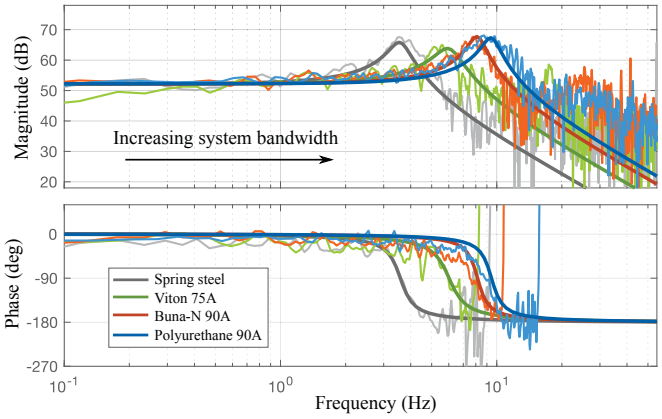


Fig. 8. **Comparison of dynamic response of four elastic elements.** Note that although the bandwidths of the four responses are different, their damping ratios (signal peak value) are relatively constant.

### E. Selection of Polyurethane 90A

In addition, a variety of other experiments were conducted to strengthen our analysis, although space prohibits us from listing those results here. Based on these results, Polyurethane 90A appears to be a strong candidate for viscoelastic actuators based on its high linearity (0.992), low compression set (2%), and low creep (15%). It is also the cheapest of the materials and comes in the largest variety of hardnesses and sizes.

## IV. SINGLE LEG TESTBED

We designed and built a single leg testbed (Fig. 1) consisting of two VLCAs - one for the ankle ($q_0$) and one for the knee ($q_1$). The design constrains motion to the sagittal plane, the leg carries $10\mathrm{kg}$ of weight at the hip, and the foot is fixed on the ground. With this testbed, we intended to demonstrate coordinated position control with two VLCAs, viability of liquid cooling on an articulated platform, cartesian position control of a weighted end effector, and verification of a linkage design. Additionally, although we will not include any force control experiments in this paper, this platform was designed with the potential to test various forms of impedance control using force feedback from the VLCAs (which we leave for future work).

The two joints each have a different linkage structure that was carefully designed so that the moment arm accommodates the expected torques and joint velocities as the leg posture changes (Fig. 9). For example, each joint can exert a peak torque of approximately 270 $\mathrm{N\,m}$ and the maximum joint velocity ranges between 7.5 $\mathrm{rad/s}$ and 20+ $\mathrm{rad/s}$ depending on the mechanical advantage of the linkage along the configurations. The joints can exert a maximum continuous torque of 91 $\mathrm{N\,m}$ at the point of highest mechanical advantage. This posture dependent ratio of torque and velocity is a unique benefit of prismatic actuators.

For the controller computational performance, we mainly rely on the quadrature encoders connected to the motor axis since the signal is far less noisy than using the joint encoders. Additionally, this strategy removes the possibility

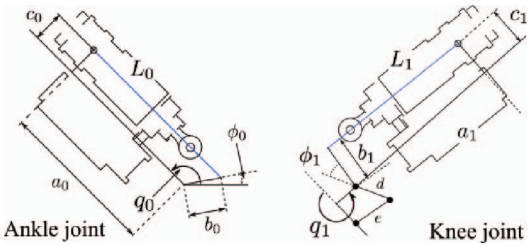


Fig. 9. **Linkage structure.** The linkages are designed to vary the maximum torque and velocity depending on the leg's posture.

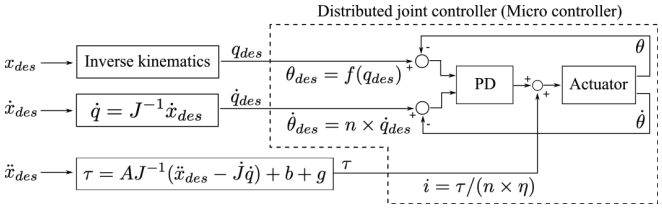


Fig. 10. **Cartesian motion control diagram.** The commands for each joint, which are a desired joint position, velocity, and torque, are converted to the motor commands. $n$ is the gear ratio and $\eta$ is the efficiency of the transmission.

of linkage backlash affecting the stability of the controller. This choice was made because we wanted to isolate the actuator performance from extraneous effects. Converting motor positions to joint positions requires nonlinear mapping functions, which we can find by solving a closed chain kinematic equation for each joint, with the assumption of negligible deflection in the elastomer elements. These derivations are omitted due to limited space.

## V. Cartesian Motion Control

Given cartesian motion trajectories, which are 2nd order B-spline or sinusoidal functions, the centralized controller computes the commands for distributed joint controllers, which are desired joint positions ($q$), velocities ($\dot{q}$), and torques ($\tau$). The commands are delivered to each embedded microcontroller. In the microcontrollers, we implement the functions converting joint positions, velocities, and torques to motor positions ($\theta$), velocities ($\dot{\theta}$), and feedforward current commands ($i$). The computation of the current commands account not only for the speed reduction ($n$) but also the approximate transmission efficiency ($\eta = 0.9$). The control diagram is shown in Fig. 10.

To obtain the desired configurations and joint velocities, we use inverse kinematics via inverse of a Jacobian matrix. Since our testbed has two DoFs and the control point is also two dimension $(x, y)$, there is a unique solution for commanded cartesian position and velocity within the joints' workspace unless the posture is singular. When we compute feedforward torque inputs, we use multi-body dynamics and an operational space control formulation.

$$\boldsymbol{A}\overline{\boldsymbol{J}}_{hip}(\ddot{\mathbf{x}} - \dot{\boldsymbol{J}}_{hip}\dot{\mathbf{q}}) + \mathbf{b} + \mathbf{g} = \boldsymbol{\tau}, \tag{1}$$

where $\boldsymbol{A}$, $\mathbf{b}$, and $\mathbf{g}$ represent inertia, coriolis, and gravity joint forces, respectively. $\dot{\mathbf{q}} \in \mathcal{R}^2$ is the joint velocity of the leg and $\tau$ is the joint torque. $\boldsymbol{J}_{hip}$ is a jacobian of the hip and $\overline{\boldsymbol{J}}_{hip}$ is a dynamically consistent pseudo inverse, which is defined as $\overline{\boldsymbol{J}} \triangleq \boldsymbol{A}^{-1}\boldsymbol{J}^{\top}(\boldsymbol{J}\boldsymbol{A}^{-1}\boldsymbol{J}^{\top})^{-1}$.

## VI. Results

In our preliminary experiments with the single leg testbed, we show: 1) the motors' core temperature behavior, 2) stable and robust motion control, and 3) achieved high mechanical power and output torque. We note that the experimental numbers presented here are smaller than the maximum power and torque that the actuators can achieve because we used fairly conservative test requirements to prevent damage to the actuators. For example, the datasheet shows maximum core temperature of the Maxon motors we use of $155$ °C, but all of our experiments were designed to maintain the motor core temperature below $90$ °C. Even with this large safety factor, our results verify that the proposed hardware can achieve both controllability and high power and torque output competitive with the state-of-art.

The experiments are performed using the single leg testbed described in Section IV and using the controller explained in Section V. Joint position data is obtained from the motor encoders depicted in Fig. 2(f). Since quadrature encoders do not provide absolute position (rather they return the incremental counts), we obtain the joint positions by synchronizing the joint position and motor position when the robot is powered on, and then accumulating the tick count from the initial positions.

### A. Continuous Power Experiment

Here, we let the hip move up and down by $0.3$ m with $1$ Hz frequency until the core temperature exceeds $80$°C. We also test the same motions without liquid cooling and compare the core temperatures of the motors. The results are shown in Fig. 11(b). The plot shows that the core temperature of the knee joint exceeds $80$ °C after $70$ s without liquid cooling; however, liquid cooled actuators remain below $80$ °C for $250$ s. Fig. 11(c) corresponds to the joint positions and velocities during a $5$ s interval. The results show that both joints stably perform position control with high accuracy.

### B. Energetics and Dynamic Motion

We test two different fast motions. In the first experiment, the leg quickly extends from a crouched posture to an extended posture during a $0.4$ s interval with zero initial and final velocities. The height change is $0.3$ m and the trajectory is parameterized by a B-spline. The maximum speed in cartesian space is $1.7$m/s and the results in Fig. 12 show that the leg performs accurate tracking behavior even during high speed movement.

The second test requires fast extension and contraction of the leg with a sinusoidal hip trajectory, also traversing $0.32$m in cartesian space, with a $2.0$ Hz frequency. The results of the fast sinusoidal motion test in Fig. 13 show that the observed maximum joint velocity is $6.1$ rad/s and the maximum observed torque is $240$N m. The torque data plot

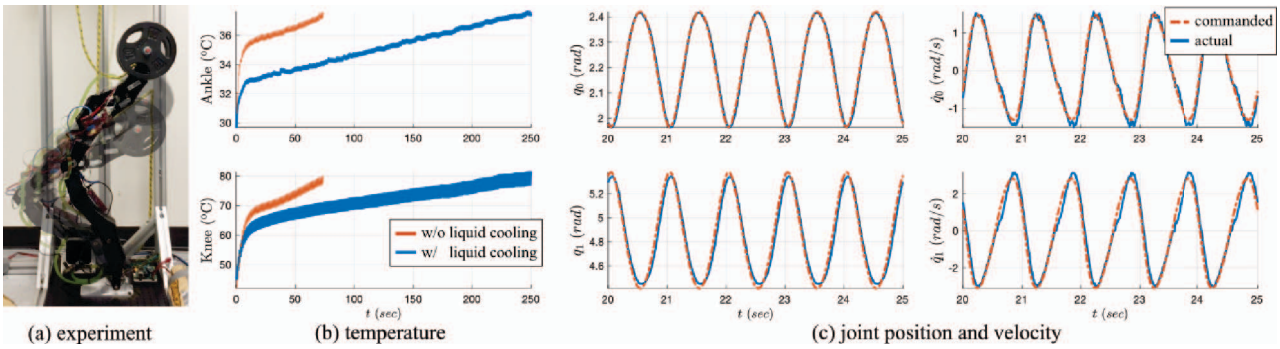


Fig. 11. **Vertical motion tests.** To test the overall performance, we let the robot move up and down by 0.3m with 1Hz frequency until the core measured motor temperature reaches 80°C. (a) corresponds to snapshots of the experiment. (b) is the temperature measurements using different cooling system (air or liquid). As we can see temperature rising is much slower with liquid cooling. (c) shows joint position and velocity data to validate accurate tracking performance.

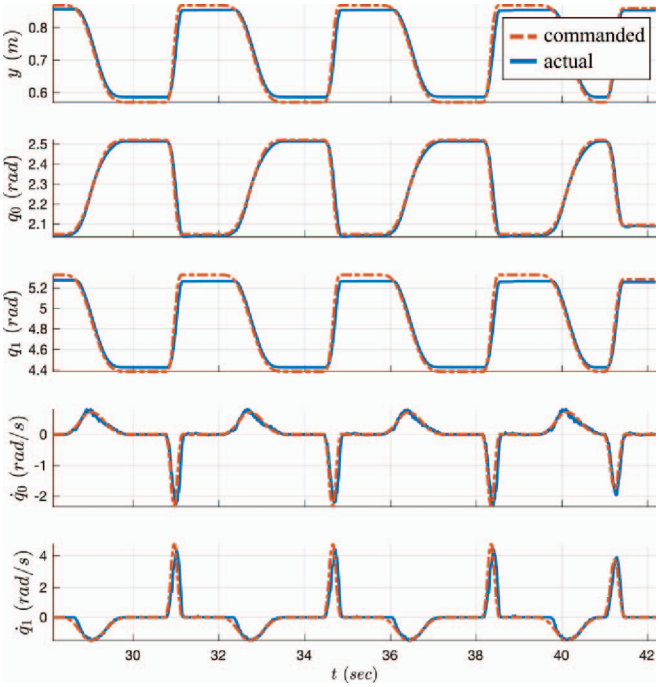


Fig. 12. **Experimental data during fast leg extension.** The leg stably and robustly achieves the high speed movements.

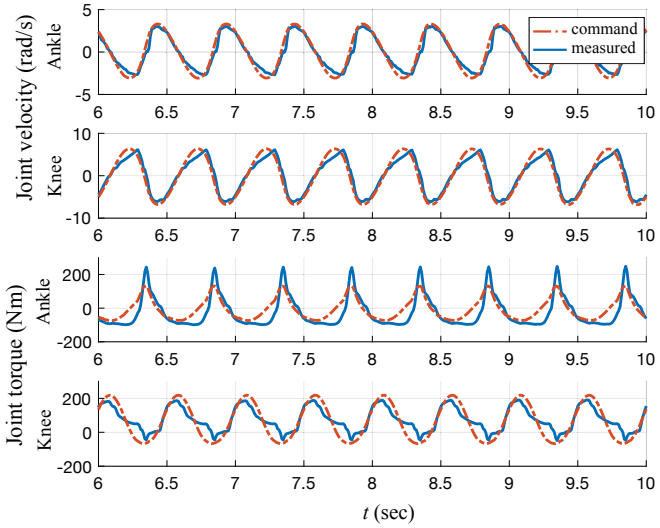


Fig. 13. **Data of fast up and down test.** The robot moves vertically by 0.32 m with frequencies of 2.0 Hz.

of Fig. 13 shows that feedforward torque used to command the motor current input and measured torque (load-cell) are similar, which means that the dynamic model we use to compute feedforward input is reasonably close to the actual system.

We wish to emphasize that the above experiments do not characterize expected empirical limits yet, but rather, establish a baseline of performance for the new actuators. By increasing the mass and/or desired speed of the movement, we believe there is significant room to increase the achievable torque and power outputs based on our currently measured motor temperatures and relative to the thermal limits and maximum rated motor currents. We decided not to test higher frequencies both due to time constraints and as a safety precaution while we mature the testing platforms.

## VII. Conclusion and Future Work

When devising the new liquid cooled viscoelastic actuation technology, we targeted high power, robust and accurate position control while protecting the drivetrain from external impact. We carefully designed the proposed actuator to satisfy various requirements for practical legged systems such as high torque and power density, high efficiency, high speed operation, and robustness to external disturbance. We have presented an experimental study with several viscoelastic materials and various key results with a single leg testbed which strongly support our performance claims. For this part of the work, we did not have the chance to try very aggressive behaviors - the testbed was only finalized a week before the submission. Our goal has been to share this early and exciting results with the humanoids community as we believe they are significant.

## Acknowledgment

The authors would like to thank the members of the Human Centered Robotics Laboratory at The University of

Texas at Austin for their great help and support. This work was supported by the Office of Naval Research, ONR Grant [grant #N000141512507] and NASA Johnson Space Center, NSF/NASA NRI Grant [grant #NNX12AM03G].

## REFERENCES


[1] I. W. Hunter, J. M. Hollerbach, and J. Ballantyne, "A comparative analysis of actuator technologies for robotics," *Robotics Review*, vol. 2, pp. 299–342, 1991.

[2] N. A. Paine, "High-performance Series Elastic Actuation," Ph.D. dissertation, Austin, 2014.

[3] A. B. Zoss, H. Kazerooni, and A. Chu, "Biomechanical design of the berkeley lower extremity exoskeleton (bleex)," *Transactions On Mechatronics*, vol. 11, no. 2, pp. 128–138, 2006.

[4] C. Semini, "Hyq-design and development of a hydraulically actuated quadruped robot," *Doctor of Philosophy (Ph. D.), University of Genoa, Italy*, 2010.

[5] C. Semini, N. G. Tsagarakis, E. Guglielmino, and D. G. Caldwell, "Design and experimental evaluation of the hydraulically actuated prototype leg of the hyq robot," in *International Conference on Intelligent Robots and Systems (IROS)*. IEEE, 2010, pp. 3640–3645.

[6] P. A. Bhounsule, J. Cortell, A. Grewal, B. Hendriksen, J. D. Karssen, C. Paul, and A. Ruina, "Low-bandwidth reflex-based control for lower power walking: 65 km on a single battery charge," *The International Journal of Robotics Research*, vol. 33, no. 10, pp. 1305–1321, 2014.

[7] N. Kanehira, T. Kawasaki, S. Ohta, T. Ismumi, T. Kawada, F. Kanehiro, S. Kajita, and K. Kaneko, "Design and experiments of advanced leg module (hrp-2l) for humanoid robot (hrp-2) development," in *International Conference on Intelligent Robots and Systems*, vol. 3. IEEE, 2002, pp. 2455–2460.

[8] I.-W. Park, J.-Y. Kim, J. Lee, and J.-H. Oh, "Mechanical design of humanoid robot platform khr-3 (kaist humanoid robot 3: Hubo)," in *5th International Conference on Humanoid Robots*. IEEE, 2005, pp. 321–326.

[9] M. Gienger, K. Loffler, and F. Pfeiffer, "Towards the design of a biped jogging robot," in *International Conference on Robotics and Automation*, vol. 4. IEEE, 2001, pp. 4140–4145.

[10] S. Lohmeier, T. Buschmann, H. Ulbrich, and F. Pfeiffer, "Modular joint design for performance enhanced humanoid robot lola," in *International Conference on Robotics and Automation*. IEEE, 2006, pp. 88–93.

[11] S. Karumanchi, K. Edelberg, I. Baldwin, J. Nash, J. Reid, C. Bergh, J. Leichty, K. Carpenter, M. Shekels, M. Gildner *et al.*, "Team robosimian: Semi-autonomous mobile manipulation at the 2015 darpa robotics challenge finals," *Journal of Field Robotics*, vol. 34, no. 2, pp. 305–332, 2017.

[12] J. Urata, Y. Nakanishi, K. Okada, and M. Inaba, "Design of high torque and high speed leg module for high power humanoid," in *International Conference on Intelligent Robots and Systems*. IEEE, 2010, pp. 4497–4502.

[13] K. Kojima, T. Karasawa, T. Kozuki, E. Kuroiwa, S. Yukizaki, S. Iwaishi, T. Ishikawa, R. Koyama, S. Noda, F. Sugai, S. Nozawa, Y. Kakiuchi, K. Okada, and M. Inaba, "Development of life-sized high-power humanoid robot JAXON for real-world use," in *15th International Conference on Humanoid Robots*. IEEE, 2015, pp. 838–843.

[14] N. Paine and L. Sentis, "Design and Comparative Analysis of a Retrofitted Liquid Cooling System for High-Power Actuators," *Actuators*, vol. 4, no. 3, pp. 182–202, 2015.

[15] F. Aghili, J. M. Hollerbach, and M. Buehler, "A modular and high-precision motion control system with an integrated motor," *Transactions on Mechatronics*, vol. 12, no. 3, pp. 317–329, 2007.

[16] F. Negrello, M. Garabini, M. G. Catalano, J. Malzahn, D. G. Caldwell, A. Bicchi, and N. G. Tsagarakis, "A modular compliant actuator for emerging high performance and fall-resilient humanoids," in *International Conference on Humanoid Robots*. IEEE, 2015, pp. 414–420.

[17] N. G. Tsagarakis, S. Morfey, G. M. Cerda, L. Zhibin, and D. G. Caldwell, "Compliant humanoid coman: Optimal joint stiffness tuning for modal frequency control," in *International Conference on Robotics and Automation*. IEEE, 2013, pp. 673–678.

[18] N. A. Radford, P. Strawser, K. Hambuchen, J. S. Mehling, W. K. Verdeyen, A. S. Donnan, J. Holley, J. Sanchez, V. Nguyen, L. Bridgwater *et al.*, "Valkyrie: Nasa's first bipedal humanoid robot," *Journal of Field Robotics*, vol. 32, no. 3, pp. 397–419, 2015.

[19] J. W. Grizzle, J. Hurst, B. Morris, H.-W. Park, and K. Sreenath, "Mabel, a new robotic bipedal walker and runner," in *American Control Conference (ACC)*. IEEE, 2009, pp. 2030–2036.

[20] A. Ramezani, "Feedback control design for marlo, a 3d-bipedal robot." 2013.

[21] M. Hutter, M. Gehring, M. Bloesch, C. D. Remy, R. Y. Siegwart, and M. A. Hoepflinger, "Starleth: A compliant quadrupedal robot for fast, efficient, and versatile locomotion," 2012.

[22] K. Abe, T. Suga, and Y. Fujimoto, "Control of a biped robot driven by elastomer-based series elastic actuator," in *2012 12th IEEE International Workshop on Advanced Motion Control (AMC)*, March 2012, pp. 1–6.

[23] Y. Zhao, N. Paine, K. Kim, and L. Sentis, "Stability and Performance Limits of Latency-Prone Distributed Feedback Controllers," *IEEE Transactions on Industrial Electronics*, vol. 62, no. 11, pp. 7151–716, November 2015.

[24] D. Lahr, V. Orekhov, B. Lee, and D. Hong, "Early developments of a parallelly actuated humanoid, saffir," in *ASME 2013 international design engineering technical conferences and computers and information in engineering conference*, 2013, pp. V06BT07A054–V06BT07A054.

[25] B. Lee, C. Knabe, V. Orekhov, and D. Hong, "Design of a Human-Like Range of Motion Hip Joint for Humanoid Robots," in *International Design Engineering Technical Conferences and Computers and Information in Engineering Conference*. American Society of Mechanical Engineers, Aug. 2014.

[26] C. Knabe, J. Seminatore, J. Webb, M. Hopkins, T. Furukawa, A. Leonessa, and B. Lattimer, "Design of a series elastic humanoid for the darpa robotics challenge," in *15th International Conference on Humanoid Robots (Humanoids)*. IEEE, 2015, pp. 738–743.

[27] J. Pratt and B. Krupp, "Design of a bipedal walking robot," in *Proc. of SPIE*, vol. 6962, 2008, pp. 69 621F1–69 621F13.

[28] J. E. Pratt, "Exploiting inherent robustness and natural dynamics in the control of bipedal walking robots," Massachusetts Inst. of Tech. Dept. of Electr. Eng. and Comp. Science, Tech. Rep., 2000.

[29] D. Kim, Y. Zhao, G. Thomas, B. R. Fernandez, and L. Sentis, "Stabilizing Series-Elastic Point-Foot Bipeds Using Whole-Body Operational Space Control," *Transactions on Robotics*, vol. 32, no. 6, pp. 1362–1379, 2016.

[30] R. Rea, C. Beck, R. Rovekamp, M. Diftler, and P. Neuhaus, "X1: A robotic exoskeleton for in-space countermeasures and dynamometry," 2013.

[31] S. Seok, A. Wang, M. Y. M. Chuah, D. J. Hyun, J. Lee, D. M. Otten, J. H. Lang, and S. Kim, "Design principles for energy-efficient legged locomotion and implementation on the mit cheetah robot," *Transactions on Mechatronics*, vol. 20, no. 3, pp. 1117–1129, 2015.

[32] N. Paine, J. S. Mehling, and J. Holley, "Actuator Control for the NASA-JSC Valkyrie Humanoid Robot: A Decoupled Dynamics Approach for Torque Control of Series Elastic Robots," *Journal of Field Robotics*, 2015.

[33] M. Hutter, C. D. Remy, M. A. Hoepflinger, and R. Siegwart, "High compliant series elastic actuation for the robotic leg scarleth," in *Proc. of the International Conference on Climbing and Walking Robots (CLAWAR)*, no. EPFL-CONF-175826, 2011.

[34] E. Pucci and G. Saccomandi, "A note on the Gent model for rubber-like materials," *Rubber chemistry and technology*, vol. 75, no. 5, pp. 839–852, 2002.